Received: 28 October 2022 | Revised: 14 April 2023 | Accepted: 28 May 2023

DOI: 10.1002/jsp2.1268

RESEARCH ARTICLE

JOR Spine OPEN ACCESS

# Novel 3D printed lattice structure titanium cages evaluated in an ovine model of interbody fusion

James W. Johnson[1] | Ben Gadomski[1] | Kevin Labus[1] | Holly Stewart[2] | Brad Nelson[2] | Howie Seim III[2] | Dan Regan[3] | Devin von Stade[1] | Cambre Kelly[4] | Phillip Horne[5] | Ken Gall[4,6] | Jeremiah Easley[2]

[1]Orthopaedic Bioengineering Research Laboratory, Colorado State University, Fort Collins, Colorado, USA

[2]Preclinical Surgical Research Laboratory, Colorado State University, Fort Collins, Colorado, USA

[3]Dept. of Microbiology, Immunology, & Pathology, Flint Animal Cancer Center, Fort Collins, Colorado, USA

[4]restor3d, Inc., Durham, North Carolina, USA

[5]Duke Health, Raleigh, North Carolina, USA

[6]Duke University, Pratt School of Engineering, Durham, North Carolina, USA

**Correspondence**
Jeremiah Easley, Preclinical Surgical Research Laboratory, Colorado State University, 2350 Gillette Dr., Fort Collins, CO 80523, USA.
Email: jeremiah.easley@colostate.edu

**Funding information**
Piedmont Society; restor3d, Inc.

## Abstract

**Background:** The use of intervertebral cages within the interbody fusion setting is ubiquitous. Synthetic cages are predominantly manufactured using materials such as Ti and PEEK. With the advent of additive manufacturing techniques, it is now possible to spatially vary complex 3D geometric features within interbody devices, enabling the devices to match the stiffness of native tissue and better promote bony integration. To date, the impact of surface porosity of additively manufactured Ti interbody cages on fusion outcomes has not been investigated. Thus, the objective of this work was to determine the effect of implant endplate surface and implant body architecture of additive manufactured lattice structure titanium interbody cages on bony fusion.

**Methods:** Biomechanical, microcomputed tomography, static and dynamic histomorphometry, and histopathology analyses were performed on twelve functional spine units obtained from six sheep randomly allocated to body lattice or surface lattice groups.

**Results:** Nondestructive kinematic testing, microcomputed tomography analysis, and histomorphometry analyses of the functional spine units revealed positive fusion outcomes in both groups. These data revealed similar results in both groups, with the exception of bone-in-contact analysis, which revealed significantly improved bone-in-contact values in the body lattice group compared to the surface lattice group.

**Conclusion:** Both additively manufactured porous titanium cage designs resulted in increased fusion outcomes as compared to PEEK interbody cage designs as illustrated by the nondestructive kinematic motion testing, static and dynamic histomorphometry, microcomputed tomography, and histopathology analyses. While both cages provided for similar functional outcomes, these data suggest boney contact with an interbody cage may be impacted by the nature of implant porosity adjacent to the vertebral endplates.

KEYWORDS
3D printing, spinal fusion, titanium cage

## 1 | INTRODUCTION

The use of intervertebral cages within an interbody fusion setting has become ubiquitous practice for treatment of degenerative disc disease. Currently, synthetic cages are predominantly manufactured using materials such as titanium and PEEK.[1] While current cages made from those materials have proven to improve stability, restore anatomically-appropriate disc height, and provide a mechanism for which to deliver osteoinductive material,[2] the lack of direct osseointegration, and elastic modulus mismatch of the cage devices provides the opportunity for complications such as subsidence[3,4] and fibrous tissue infiltration.[5] The inability to form direct osseointegration results from the traditional manufacturing methods employed, being constrained to utilizing relatively solid 2D surfaces. However, with the advent of additive manufacturing techniques the past decade, it is now possible to implement 3D geometric features in a spatially varied manner.[6,7] As such, it can be imagined that by tailoring the body geometry and porosity of an intervertebral cage, bony integration with the vertebral endplates could be achieved, improving clinical outcomes, earlier time to fusion, and patient satisfaction. While these capabilities enable new and exciting designs,[8–10] the impact of these features on bony fusion are not well studied in preclinical models.

Thus, the objective of this preliminary study was to determine the effect of implant endplate surface and implant body architecture of additive manufactured lattice structure titanium interbody cages on bony fusion in an ovine model using biomechanical, radiographic, and histological assessment techniques. We hypothesized that the increased interbody cage surface area adjacent to the vertebral endplates of the additively manufactured titanium interbody cages would drive improved osseointegration outcomes as compared to predicate PEEK cage devices.

## 2 | MATERIALS AND METHODS

This study was performed under approval from the Colorado State University Institutional Animal Care and Use Committee (#1447). Six skeletally mature (3–5 years of age; 65–115 kg) Rambouillet Cross (*Ovis aries*) ewes underwent bilevel lumbar interbody fusion using either a body lattice design (restor3d Inc., Durham, NC; Figure 1A) or body plus surface lattice design (restor3d Inc., Durham, NC; Figure 1B) interbody cage. The overall geometry of both implants was identical (22 × 14 × 8/0.55 $cm^3$ aperture volume, 75% porosity), and both designs include a sheet-based gyroid lattice with open porous structure, and in the surface lattice, an additional surface porous layer of 0.5 mm thickness of smaller gyroid at the endplates of the implant. Both implants were manufactured using spherical 30-micron Ti6Al4V ELI powder (in compliance with ASTM F3001), generating implants with surface roughness of ~7 µm as measured by optical profilometry techniques. As described previously,[11] Penicillin PPG (10 cc, 20 000 units/kg, subcutaneous [SQ]), buprenorphine (0.01 mg/kg, SQ), Phenylbutazone (1 g, oral [PO]), and two fentanyl patches (100 and 50 mcg, transdermal) were administered to all ewes 24 h prior to surgery and persisted for 5 days following surgery. While under general anesthesia, ewes were placed in right lateral recumbency. A left lateral retroperitoneal approach was utilized to dissect the oblique abdominal muscles and

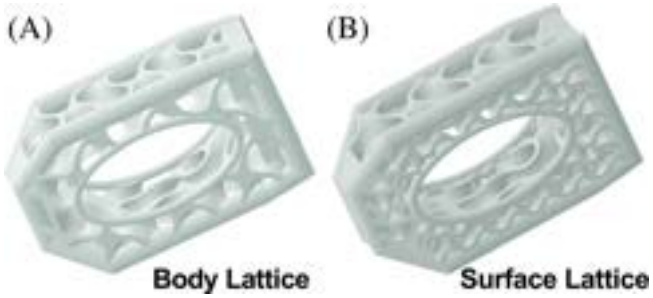


**FIGURE 1** Illustrations of body lattice (A) and surface lattice (B) cage geometry.

expose the L2 through L5 vertebra. Pituitary rongeurs were utilized to remove the annulus fibrosis and nucleus pulposus following annulotomies on the L2–L3 and L4–L5 intervertebral discs. Preparation of the vertebral endplates was accomplished following distraction of the intervertebral space, followed by progressing a 6 mm drill bit through the disc space to remove any additional annulus or nucleus material. Final removal of soft tissue and preparation of the endplates was performed using a 6.5 mm diamond burr to create an interbody defect that would accommodate the interbody implant. Cage designs were alternated between consecutive animals, with each animal receiving the body lattice cage (Figure 1A) on one level and the surface lattice (Figure 1C) on the other operated level. Prior to implantation, the center graft windows of the interbody cages were packed with morselized autograft bone obtained from the iliac crest. Following cage implantation, 4.5 mm × 30 mm polyaxial pedicle screws (ArcasUltra™, ArteMedics, Minneapolis, MN) were inserted in the cranial and caudal vertebral bodies in the dorsal plane and secured with precut 5.5 mm × 80 mm titanium rods and locking caps (ARCAS-003, ArteMedics, Minneapolis, MN). Following recovery, ewes were permitted to ambulate and eat ad libitum. Throughout the course of the study, ewes were checked daily for signs of neurological deficits, ambulatory status, pain, infection, and any other signs of complications.

Two fluorochrome labels were administered to enable subsequent dynamic histomorphometry analysis (Calcein green, 8-weeks prior to sacrifice, IV 15 mg/mL, 10 mg/kg; Xylenol orange, 4-weeks prior to sacrifice, IV 90 mg/mL, 80 mg/kg). All sheep were humanely euthanized at 16-weeks postsurgery. Functional spinal units (FSUs) were dissected from the lumbar spine sections for ex vivo analyses. Care was taken to maintain the integrity of structural soft tissues including the facet capsular ligaments, anterior and posterior longitudinal ligaments, interspinous ligaments, and supraspinatus ligaments. The polyaxial pedicle screws and associated hardware were removed, and sample hydration was preserved with phosphate buffered saline during the dissection and subsequent biomechanical testing phases.

### 2.1 | Nondestructive biomechanical testing

Nondestructive kinematic testing was performed on all operated FSUs.[12–14] To enable grasping of the samples within the spine testing system, the cranial and caudal segments from each FSU were mounted in a

two-part hardening resin (SmoothCast 321, Smooth-On, Macungie, PA). A custom spine testing system utilizing a stepper motor actuator (Model: E1402000E701, Danaher Controls, Gurnee, IL) in a force-feedback loop with a separate torque sensor was utilized to test the samples. Pure moment loading was applied to the samples and measured with a six degree-of-freedom load transducer (AMTI, Watertown, MA). A four-camera stereophotogrammetry system (Motion Analysis Corp., Santa Rosa, CA) was utilized to measure the relative spinal motion in three-dimensions during testing. This was accomplished through tracking of optical marker triads mounted to Kirschner wires that were secured in the cranial and caudal FSUs. FSUs underwent five cycles of loading, and the final cycle was used to measure the standard spinal fusion kinematic output parameters [i.e., range of motion (ROM, deg), neutral zone (NZ, deg), neutral zone stiffness (NZ stiffness, Nm/deg), and elastic zone stiffness (EZ stiffness, Nm/deg)] in all three principal directions (i.e., flexion/extension, lateral bending, and axial rotation). ROM was computed as the absolute difference between the maximum and minimum rotational angles. The NZ limits were defined at the locations where the second derivative of the angle were maximum and minimum, with the NZ being defined as the difference between those respective values. The NZ stiffness was computed as the inverse of the slope of the moment-rotation curve within the NZ range. The EZ stiffness was defined as the inverse of the slope of the moment-rotation curve at the maximum and minimum tested moments. The testers were blinded to treatment group during dissection and computation of kinematic output parameters. Upon completion of biomechanical testing, samples were placed in 10% neutral buffered formalin for fixation.

### 2.2 | Microcomputed tomography

Following completion of the nondestructive biomechanical testing, samples underwent microcomputed tomography (μCT) scanning. The region of interest scanned for each specimen included both vertebral body endplates, the interbody cages, and all osseous tissue surrounding the disc/fusion space. Scans were completed using the following settings: isotropic resolution, 37 μm; voltage, 70 kVp; current, 114 μA; and integration time, 500 ms (Scanco μCT 80, Scanco USA Inc., Wayne, Pennsylvania). The region of interest (ROI) for all samples was defined by the exterior faces of the interbody cages. Bone volume fraction (BV/TV, %) and bone mineral density (BMD, mg HA/ccm) were calculated for all specimens. BV/TV was calculated by normalizing the bone volume to the total volume less the cage volume.

### 2.3 | Histology and histomorphometry

Following μCT scanning and complete sample fixation, undecalcified histological slides were produced from each sample. Histological sections were taken in the sagittal plane through the device to display the implant's core, the implant's anterior and posterior surfaces (i.e., walls), and the surrounding bone. Subsequently, samples were dehydrated in graded solutions of ethanol and cleared with methyl salicylate and xylene. Samples were then infiltrated and polymerized into a hardened block (Acrylosin Hard, Dorn and Hart Microedge Inc., Loxley, AL). Two slides were cut from each FSU using the EXAKT Cutting and Grinding system (EXAKT Technologies Inc., Oklahoma City, OK). One slide was stained with Sanderson's rapid bone stain with a subsequent Van Gieson's counterstain. The second slide was left unstained for dynamic histomorphometry analysis.

Calibrated digital images of stained and unstained slides were taken using a Nikon E800 microscope at 10× and 40× magnification, respectively (ImagePro, Media Cybernetics, Silver Spring, MD). Image settings were optimized and remained consistent for all slides. For static histomorphometry measurements, the ROI was defined by the exterior surfaces of the interbody cages (i.e., cage material and inside lumen). Within this ROI, percent bone area (BA, %), percent fibrous tissue area (FA, %), and percent void area (VA, %) were quantified after subtracting the implant area. Additionally, the percent bone in contact (BIC, %) with the interbody cage material was calculated by quantifying the length of bone in contact with cage material and normalizing to the circumference of the cage material present on the histology slide. Dynamic histomorphometry measurements were made across three ROIs for each sample and included cranial endplate area, interbody cage lumen area, and caudal endplate area. The mean of the values measured at the cranial and caudal endplate areas was reported as the endplate ROI. Across all ROIs, mineralized surface (MS, %), mineral apposition rate (MAR, μm/day), and bone formation rate (BFR, μm/day) were quantified.[15] A board-certified veterinary pathologist evaluated stained histology slides using a semiquantitative scale to assess cell types (polymorphonuclear cells, lymphocytes, plasma cells, macrophages, giant cells, and osteoblasts), responses (bone remodeling, implant degradation, and neovascularization), and bony bridging. All histomorphometry and histopathology assessments were made by a blinded reviewer who was unblinded only for data postprocessing.

### 2.4 | Statistical analysis

Nondestructive biomechanical outcome data from Empty and Autograft PEEK cages (TECAPEEK CLASSIX, Artemedics, Inc.) prepared and tested identically to these samples are redisplayed in Figures 2 and 3.[11] Following confirmation of normal distribution of all data via Shapiro–Wilk test, statistical comparisons were made using a two-tailed paired *t*-test on all continuous data (i.e., biomechanical, μCT, static and dynamic histomorphometry data). The significance threshold ($\alpha$) was equal to 0.05.

## 3 | RESULTS

Surgery was completed consistently and without intraoperative complication across all animals. No unexpected abnormalities were noted following surgery and all animals survived to the study endpoint.

### 3.1 | Nondestructive biomechanical testing results

All biomechanical tests were run to completion. The Body Lattice titanium cage group exhibited significantly increased lateral

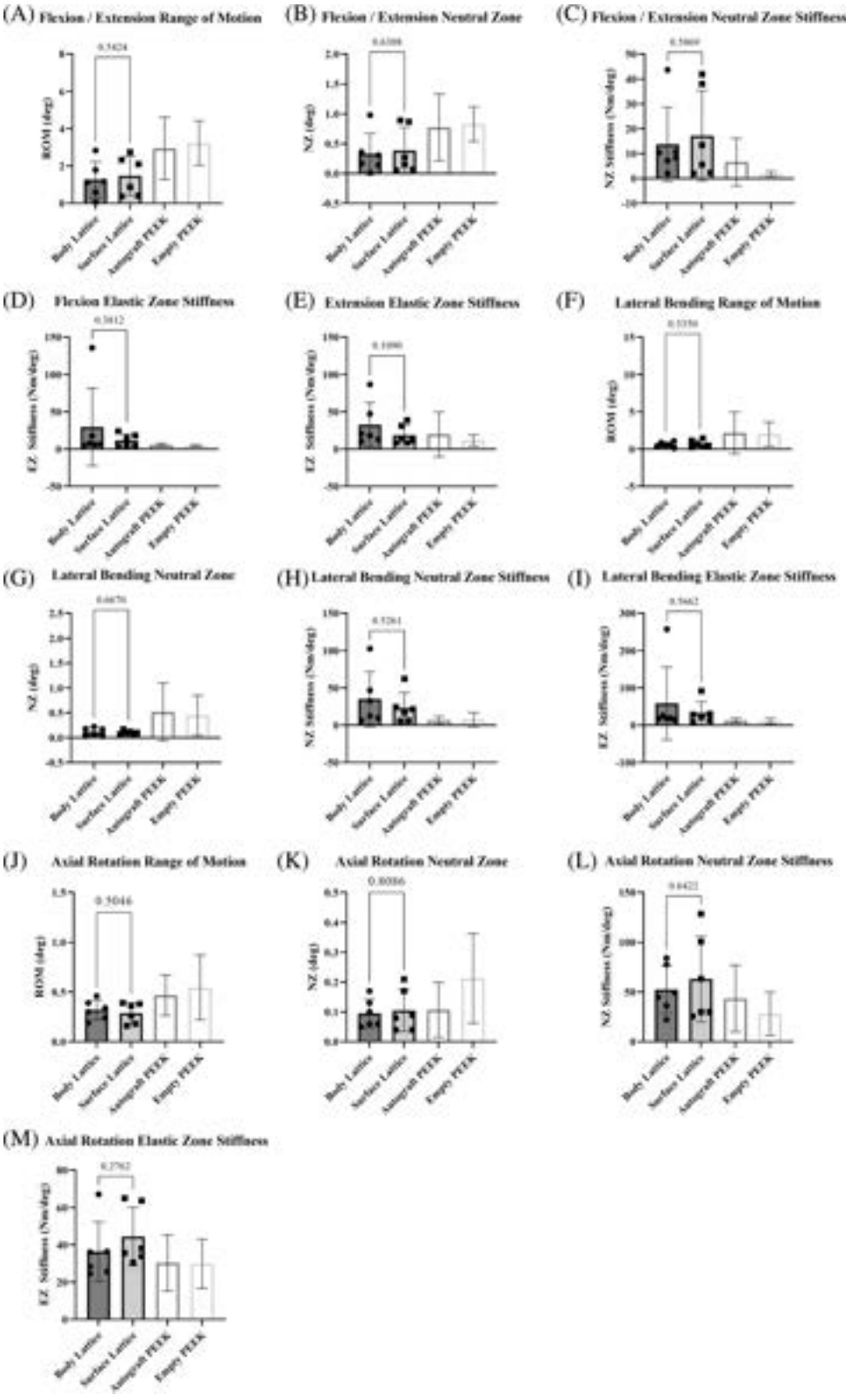


**FIGURE 2** Nondestructive biomechanical testing results. (A–E) Flexion-extension direction testing range of motion (ROM), neutral zone (NZ), NZ stiffness, and elastic zone (EZ) stiffness. (F–I) Lateral bending direction testing ROM, NZ, NZ stiffness, and EZ stiffness. (J–M) Axial rotation direction testing ROM, NZ, NZ stiffness, and EZ stiffness. Autograft PEEK and Empty PEEK groups data from Gadomski et al. 2021.

bending NZ stiffness as compared to the Autograft PEEK group ($p = 0.050$). No significant differences between groups in the other biomechanical outcome parameters were noted (Figure 2A–M).

## 3.2 | Microcomputed tomography

While no significant differences in microCT outcome parameters between the two implant designs were noted, microCT analysis

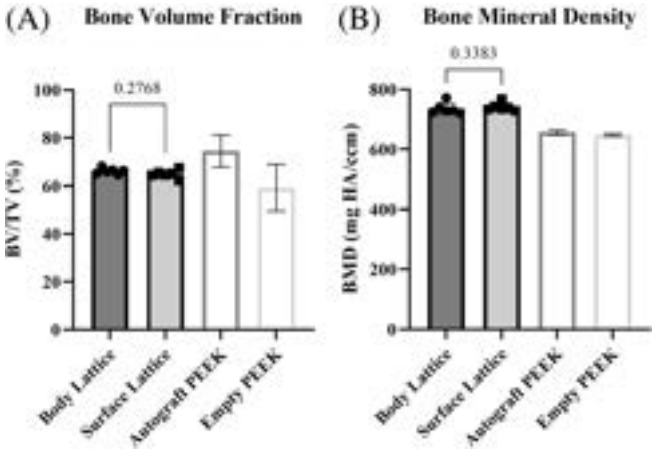


**FIGURE 3** Quantitative μCT analysis results. (A) No significant differences were noted in bone volume fraction between cage designs. (B) Bone mineral density was not significantly different between cage groups. Bar charts illustrate mean and whiskers illustrate standard deviations. Autograft PEEK and Empty PEEK groups data from Gadomski et al. 2021.

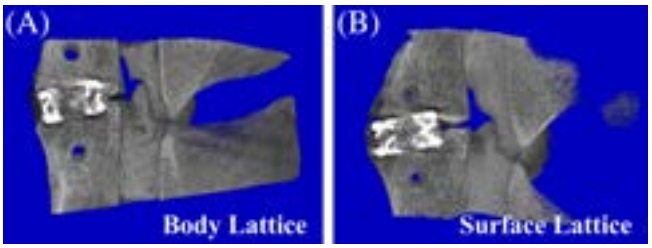


**FIGURE 4** Representative sagittal plane three-dimensional μCT reconstruction images of the implanted body lattice (A) and surface lattice (B) cage designs.

revealed positive fusion characteristics in both cage designs as evidenced by BV/TV ($p = 0.18$, Figure 3A) and BMD ($p = 0.63$, Figure 3B) measurements. Representative cross-sectional images of the implanted Body Lattice and Surface Lattice titanium cages in the sagittal plane are included in Figure 4.

## 3.3 | Histology and histomorphometry

Static histomorphometry analyses demonstrated positive fusion characteristics in both cages designs; however, significant differences between cage designs were not found in percent bone area ($p = 0.36$, Figure 5A), percent fibrous tissue area ($p = 0.41$, Figure 5B), nor percent empty area ($p = 0.39$, Figure 5C). However, analyses did reveal marginally improved percent bone in contact within the body lattice group as compared to the surface lattice group ($p = 0.03$, Figure 5D). Additionally, the cage designs did not impact fusion outcome as evidenced by the dynamic histomorphometry outcome parameters (e.g., mineralizing surface, mineral apposition rate, and bone formation rates, Table 1).

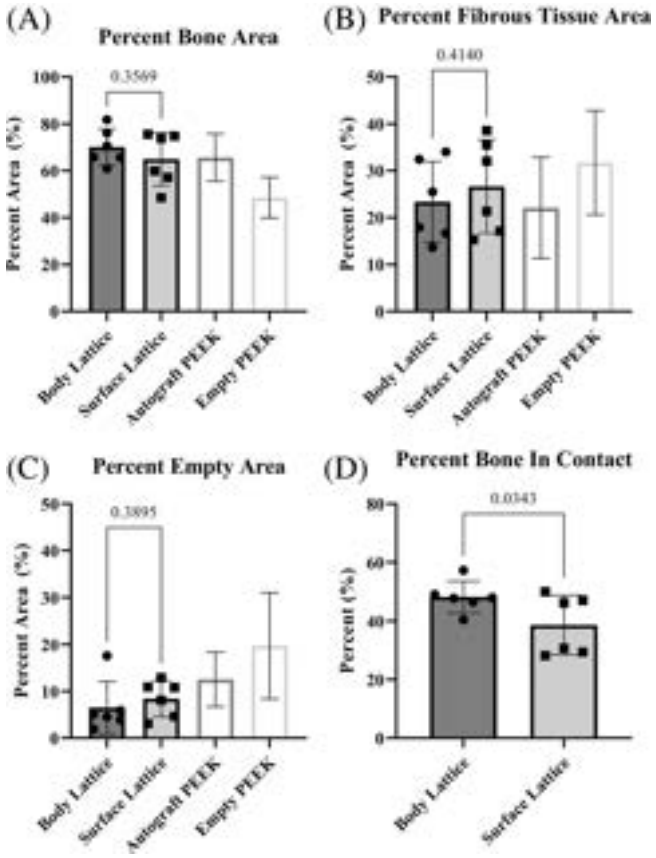


**FIGURE 5** Static histomorphometry analysis results. No significant differences were noted in percent bone area (A), percent fibrous tissue area (B), or percent empty area (C) between cage designs. The Body Lattice group exhibited significantly increased percent bone in contact as compared to the Surface Lattice group. Bar charts illustrate mean and whiskers illustrate standard deviations. Autograft PEEK and Empty PEEK groups data from Gadomski et al. 2021.

## 3.4 | Histopathology

Representative micrographs of both cage designs are included in Figure 6. Both cage design groups exhibited new bone formation and complete union between the vertebral endplates. Specifically, new bone formed within the cage lumen space was composed of variably thick, densely packed trabeculae composed primarily of remodeled mature lamellar bone with modest amounts of woven bone. Across both cage design groups, mild osteoblast activity was observed along new bone surfaces for all sections, and rare, mild osteoclast activity in some sections in areas of active remodeling. Areas of greatest activity were generally at the junction of woven and lamellar bone where trabecular surfaces of new bone were lined by a single dense layer of plump osteoblasts with rare, nearby osteoclasts within Howship's lacunae.

The local inflammatory response surrounding the implant was minimal, often represented by low numbers of lymphocytic or histiocytic infiltrates with equivocal levels between treatment groups. These infiltrates were concentrated in the fibrous connective tissue

| Outcome parameter | Body lattice | Surface lattice | *p* value |
|---|---|---|---|
| Endplate ROI: Mineralizing surface | 22.8 ± 5.8 | 24.9 ± 2.6 | 0.44 |
| Endplate ROI: Mineral apposition rate | 1.62 ± 0.18 | 1.69 ± 0.33 | 0.76 |
| Endplate ROI: Bone formation rate | 0.39 ± 0.12 | 0.43 ± 0.07 | 0.98 |
| Central ROI: Mineralizing surface | 20.7 ± 9.5 | 20 ± 9.7 | 0.90 |
| Central ROI: Mineral apposition rate | 1.74 ± 0.55 | 1.48 ± 0.43 | 0.48 |
| Central ROI: Bone formation rate | 0.44 ± 0.11 | 0.36 ± 0.16 | 0.39 |

**TABLE 1** Histomorphometry outcome parameters. No significant differences were noted between cage designs. Values are reported as means ± SD.

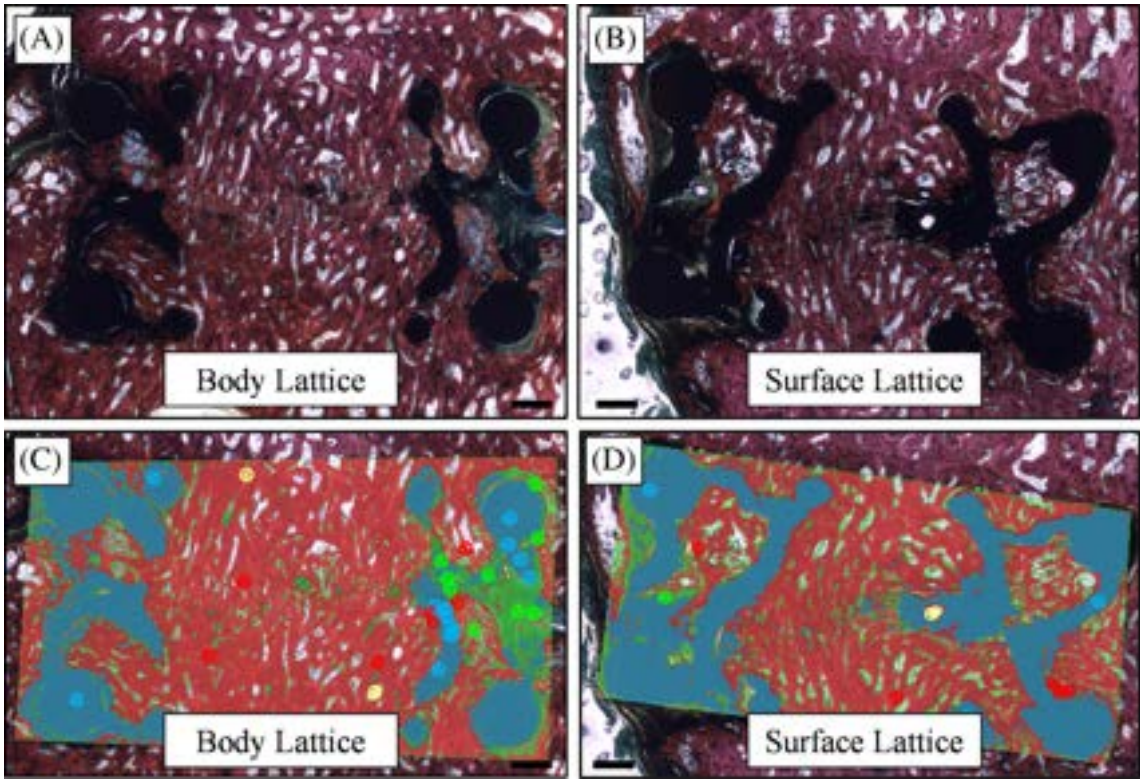


**FIGURE 6** Representative micrographs of the (A) body lattice and (B) surface lattice cage designs exhibiting complete fusion across the disc space and lack of peri-implant fibrotic growth. Matching histomorphometry segmentation images of the (C) body lattice and (D) surface lattice designs are shown with red representing bone area, blue as implant area, and green as fibrous tissue area. Scale bars are 1 mm.

surrounding areas of the implant and could be consistent with an appropriate host tissue response to postoperative remodeling. Other soft tissue changes (i.e., fibrosis, neovascularization) were not different between cage design groups. In areas in proximity to remnant annulus, some fibrosis was noted and manifested as dense fibrous connective tissue intimately surrounding the implant. Neovascularization was observed primarily within the aforementioned fibrotic tissue, with no difference between cage design groups.

## 4 | CONCLUSIONS

As evidenced by biomechanical testing, static and dynamic histomorphometry, microCT, and histopathological analyses, both additively manufactured titanium cage designs yielded positive fusion outcomes. While significant differences in outcome parameters between titanium cage design groups were not found, qualitative comparisons with a previously published study that utilized PEEK cages highlight the difference of fusion quality between these two cage materials. Specifically, the nondestructive biomechanical testing data revealed greatly improved fusion performance in the lateral bending and flexion/extension directions of both titanium cage groups as compared to the PEEK cage with or without Autograft samples from a previous study.[11] The microCT analysis revealed improved bone mineral density in the titanium cage design groups as compared to both PEEK groups.[11] Additionally, the titanium cage design groups exhibited improved bone volume fraction as compared to the Empty PEEK group. The histomorphometry analysis also revealed improved fusion outcomes in the titanium cage groups as compared to the PEEK cage groups, with increased percent bone area and decreased empty

area.[11] When taken together, these data illustrate the superior boney integration of additively manufactured porous titanium interbody cages as compared to solid PEEK interbody cages. Again, in contrast to previous studies utilizing PEEK interbody cages,[8,14] both additively manufactured porous titanium interbody cage groups exhibited high percentages of bone-in-contact, as well as minimal fibrous tissue area within the cage area. Qualitatively, the fusion exhibited by the titanium cage samples was further progressed at the same time point as compared to the PEEK cages. This was manifested through more complete trabecular remodeling and a fusion mass that completely filled the cage lumen in the titanium samples; whereas the PEEK samples had some gapping in the cranial/caudal center plane of the lumen where the fusion had not yet completed.

In comparing the performance of the titanium cage designs, it is evident that altering the porous architecture of the interbody cage near the endplate region does not greatly impact functional fusion outcomes. However, the surface lattice cage group exhibited a 19.8% decrease ($p = 0.077$) in bone in contact values, suggesting that porosity can possibly impact osseointegration. Moreover, there was no significant difference observed between the bone formation behavior or rates in the central aperture versus the latticed endplate regions of either implant design, indicating bone formation occurs through the endplates of the implant in parallel to fusion of the central aperture. We note that in a clinical setting surface porosity may be added to a porous 3d printed metal cage to help mitigate cage subsidence.

While PEEK interbody cages have been utilized clinically, their inert nature leads to a lack of direct osseointegration of those implants in the absence of porosity.[14,16] Porous titanium implants overcome this shortfall, enabling improved bonding with bone; however, the high stiffness of solid titanium interbody cages exceeds that of bone, reducing fusion outcomes.[12,17] The advent of additively manufactured titanium cages with tailored geometry and stiffness values has been proven to lead to successful fusion outcomes.[8,9] Data presented here agree with previous studies and exhibit the positive fusion potential of additively manufactured titanium cages. This preliminary study reports the fusion outcomes of an ovine model of interbody fusion; as such, consideration should be exercised when translating these results to human. Additionally, the small sample size limits the power of these data. While titanium implants are widely used and accepted within the orthopedic field, there is concern that increasing surface area may present a risk of corrosion/metal ion release. While no evidence of corrosion or metal ion release was noted during this study, this study was not designed to assess those phenomena.

In summary, both additively manufactured porous titanium cage designs resulted in increased fusion outcomes as compared to previously published PEEK interbody cage designs as illustrated by the nondestructive kinematic motion testing, static and dynamic histomorphometry data, μCT, and histopathology analyses. While both cages provided for similar functional outcomes, these data suggest boney contact with an interbody cage may be impacted by the nature of implant porosity adjacent to the vertebral endplates.

## AUTHOR CONTRIBUTIONS

All authors contributed to all aspects of this manuscript. All authors have read and approved the final version of this manuscript.

## ACKNOWLEDGMENTS

This work was funded by a research grant from the Piedmont Society (Duke University Medical Center; Durham, NC) and restor3d, Inc., (Durham, NC).

## FUNDING INFORMATION

This work was funded by support from the Piedmont Orthopedic Foundation and restor3D.

## CONFLICT OF INTEREST STATEMENT

C.K. and K.G. are paid employees of restor3d, Inc. P.H. is a paid consultant of restor3d, Inc. The authors have no conflict of interest.

## ORCID

*James W. Johnson* https://orcid.org/0000-0001-7465-3854
*Ben Gadomski* https://orcid.org/0000-0003-1434-0551

## REFERENCES

1. Seaman S, Kerezoudis P, Bydon M, Torner JC, Hitchon PW. Titanium vs. polyetheretherketone (PEEK) interbody fusion: meta-analysis and review of the literature. *J Clin Neurosci*. 2017;*44*:23-29.
2. Blumenthal SL, Ohnmeiss DD. Intervertebral cages for degenerative spinal diseases. *Spine J*. 2003;*3*:301-309.
3. Lee JH, Jeon DW, Lee SJ, Chang BS, Lee CK. Fusion rates and subsidence of morselized local bone grafted in titanium cages in posterior lumbar interbody fusion using quantitative three-dimensional computed tomography scans. *Spine (Phila Pa 1976)*. 2010;*35*:1460-1465.
4. Vaidya R, Sethi A, Bartol S, Jacobson M, Coe C, Craig JG. Complications in the use of rhBMP-2 in PEEK cages for interbody spinal fusions. *Clin Spine Surg*. 2008;*21*:557-562.
5. Noordhoek I, Koning MT, Jacobs WCH, Vleggeert-Lankamp CLA. Incidence and clinical relevance of cage subsidence in anterior cervical discectomy and fusion: a systematic review. *Acta Neurochir*. 2018;*160*:873-880.
6. Tack P, Victor J, Gemmel P, Annemans L. 3D-printing techniques in a medical setting: a systematic literature review. *Biomed Eng Online*. 2016;*15*:115.
7. Kelly CN, Francovich J, Julmi S, et al. Fatigue behavior of As-built selective laser melted titanium scaffolds with sheet-based gyroid microarchitecture for bone tissue engineering. *Acta Biomater*. 2019;*94*:610-626.
8. Loenen ACY, Peters MJM, Bevers RTJ, et al. Early bone ingrowth and segmental stability of a trussed titanium cage versus a polyether ether ketone cage in an ovine lumbar interbody fusion model. *Spine J*. 2022;*22*:174-182.
9. Fogel G, Martin N, Lynch K, et al. Subsidence and fusion performance of a 3D-printed porous interbody cage with stress-optimized body lattice and microporous endplates – a comprehensive mechanical and biological analysis. *Spine J*. 2022;*22*:1028-1037.
10. Kelly CN, Evans NT, Irvin CW, Chapman SC, Gall K, Safranski DL. The effect of surface topography and porosity on the tensile fatigue of 3D printed Ti-6Al-4V fabricated by selective laser melting. *Mater Sci Eng C*. 2019;*98*:726-736.
11. Gadomski BC, Labus KM, Puttlitz CM, et al. Evaluation of lumbar spinal fusion utilizing recombinant human platelet derived growth

factor-B chain homodimer (rhPDGF-BB) combined with a bovine collagen/β-tricalcium phosphate (β-TCP). *JOR Spine*. 2021;*4*:e1166.
12. McGilvray KC, Waldorff EI, Easley J, et al. Evaluation of a polyetheretherketone (PEEK) titanium composite interbody spacer in an ovine lumbar interbody fusion model: biomechanical, microcomputed tomographic, and histologic analyses. *Spine J*. 2017;*17*:1907-1916.
13. Easley J, Puttlitz CM, Seim H, et al. Biomechanical and histologic assessment of a novel screw retention technology in an ovine lumbar fusion model. *Spine J*. 2018;*18*:2302-2315.
14. McGilvray KC, Easley J, Seim HB, et al. Bony ingrowth potential of 3D-printed porous titanium alloy: a direct comparison of interbody cage materials in an in vivo ovine lumbar fusion model. *Spine J*. 2018;*18*:1250-1260.
15. Dempster DW, Compston JE, Drezner MK, et al. Standardized nomenclature, symbols, and units for bone histomorphometry: a 2012 update of the report of the ASBMR Histomorphometry Nomenclature Committee. *J Bone Miner Res*. 2013;*28*:2-17.
16. Yoon BJV, Xavier F, Walker BR, Grinberg S, Cammisa FP, Abjornson C. Optimizing surface characteristics for cell adhesion and proliferation on titanium plasma spray coatings on polyetheretherketone. *Spine J*. 2016;*16*:1238-1243.
17. Chen Y, Wang X, Lu X, et al. Comparison of titanium and polyetheretherketone (PEEK) cages in the surgical treatment of multilevel cervical spondylotic myelopathy: a prospective, randomized, control study with over 7-year follow-up. *Eur Spine J*. 2013;*22*:1539-1546.

**How to cite this article:** Johnson, J. W., Gadomski, B., Labus, K., Stewart, H., Nelson, B., Seim, H. III, Regan, D., von Stade, D., Kelly, C., Horne, P., Gall, K., & Easley, J. (2023). Novel 3D printed lattice structure titanium cages evaluated in an ovine model of interbody fusion. *JOR Spine*, *6*(3), e1268. https://doi.org/10.1002/jsp2.1268